

Rheo-PIV analysis of the slip flow of a metallocene linear low-density polyethylene melt

Francisco Rodríguez-González ·
José Pérez-González · Lourdes de Vargas ·
Benjamín M. Marín-Santibáñez

Received: 25 June 2009 / Accepted: 13 November 2009 / Published online: 3 December 2009
© Springer-Verlag 2009

Abstract The continuous extrusion of a metallocene linear low-density polyethylene through a transparent capillary die with and without slip was analyzed in this work by rheometrical measurements and particle image velocimetry (PIV). For this reason, a comparison was made between the rheological behaviors of the pure polymer and blended with a small amount of fluoropolymer polymer processing additive. Very good agreement was found between rheometrical and PIV measurements. The pure polymer exhibited stick-slip instabilities with nonhomogeneous slip at the die wall, whereas the blend showed stable flow. The slip velocity was measured directly from the velocity profiles and was negligible for the pure polymer before the stick-slip but increased monotonously as a function of the shear stress for the blend. The flow curves and the slip velocity as a function of the shear stress deviated from a power law and were well fitted by continuous “kink” functions. Comparison of PIV data with rheometrical ones permitted a direct proof of the basic assumption of the Mooney theory. Finally, the analysis of the velocity profiles showed that there is a maximum in

the contribution of slip to the average fluid velocity, which is interpreted as the impossibility for the velocity profile to become plug like in the presence of shear thinning.

Keywords PIV · Slip velocity · Extrusion · Polyethylene · Metallocene

Introduction

Flow enhancement or slip in polymeric liquids has been documented for a long time, starting with the work by some of the pioneers in Rheology (Mooney 1931; Reiner 1931). Flow enhancement has been associated with a failure of the zero-velocity condition (no-slip) for a fluid at a solid boundary and has received particular attention due to its relevance for rheometry and materials processing (see the works by Joshi et al. 2000; Denn 2001 and Malkin 2006 for reviews). Different types of flow enhancement have been recognized, which may be roughly divided into “true” and “apparent” slip, whether the no-slip condition really fails or not. A description of the different types of slip occurring in polymer melt flows was provided by El Kissi and Piau (1996).

The presence of slip in the flow of polymer melts was sometimes related to the appearance of flow instabilities. However, it is known now that strong slip permits the elimination of stick-slip instabilities and extrudate distortions in the flow of polymer melts. Strong slip conditions may be attained by the use of low-surface energy coatings in extrusion dies (Piau et al. 1995a, b; Wang 1999; Migler et al. 2001), as well as with some

Three of us dedicate our contribution in this work to Prof. Lourdes de Vargas, our always encouraging mentor and friend, on occasion of her retirement from Instituto Politécnico Nacional.

F. Rodríguez-González · J. Pérez-González (✉) ·
L. de Vargas · B. M. Marín-Santibáñez
Laboratorio de Reología, Escuela Superior de Física y
Matemáticas, Instituto Politécnico Nacional, Apdo. Postal
118-209, C. P. 07051, México D. F., México
e-mail: jpg@esfm.ipn.mx

dies made up of high-surface energy alloys, like brass or other copper alloys (Ramamurthy 1986; Ghanta et al. 1999; Pérez-González and Denn 2001).

Although the slip phenomenon has been invoked in many works related with the extrusion of polymer melts, its manifestation is far from the observed under true strong slip conditions. For example, many works reporting slip in linear polyethylenes still show extrudate sharkskin distortions and non-monotonic flow curves (stick-slip flow). In contrast, extrusion under strong slip conditions produces outstanding macroscopic phenomena as elimination of sharkskin, monotonic flow curves (no stick-slip), and electrification of the melt (Ghanta et al. 1999; Pérez-González and Denn 2001; Migler et al. 2001; Pérez-González 2001).

Most reports about flow enhancement in polymer melts include the calculation of the slip velocity (v_s) from rheometrical data by using the method proposed by Mooney (1931), with almost no reference to the underlying flow kinematics. The slip velocity has been typically reported as a power law function of the shear stress, a model that is often used in numerical calculations (Denn 2001; Malkin 2009). Also, there is still the belief that the velocity profile becomes plug like in the presence of slip flow. These two issues, however, are still not fully corroborated. In fact, more complex slip velocity versus shear stress relationships have been proposed, some of them for instance, suggesting a maximum in the slip velocity (Leonov 1990; Piau and El Kissi 1994), and there is not evidence for fully plug-like velocity profiles obtained under slip flow conditions of polymer melts.

In spite of the large amount of publications in the field, only a few works have been devoted to the analysis of the slip kinematics by using velocimetry techniques. Müller-Mohnssen et al. (1987) measured the velocity profiles for polyacrylamide solutions by using laser Doppler velocimetry (LDV) and found evidence of apparent slip, this being originated by a depleted polymer layer. Later, Rofe et al. (1996) determined the velocity profiles for aqueous xanthan solutions by means of nuclear magnetic resonance imaging. These authors also reported evidence of apparent slip and proved the validity of the Mooney method.

Regarding the flow of molten polymers, Atwood and Schowalter (1989) used a hot probe technique to measure the velocity of high-density polyethylene (HDPE) in a slit die and concluded that the flow was almost plug-like during the stick-slip. Piau et al. (1995a) carried out LDV in a polybutadiene flowing through a slit channel and showed that slip, characterized by a nearly plug flow, occurred when the die surface was fluorinated.

Münstedt et al. (2000) reported what is probably the first description of the velocity profiles during the slit flow of HDPE by using LDV. Even though their work was limited to a narrow shear rate range, these authors described the typical characteristics of the velocity profiles in the three regimes of the unstable flow curve. Later, Migler et al. (2001) developed a rheo-optics technique to visualize how polymer processing additives (PPA) eliminate sharkskin in linear low-density polyethylene (LLDPE). These authors measured the velocity profiles and the coating process of PPA in a sapphire capillary and showed evidence of slip in the coated die and adhesion when this was uncoated. A more detailed description of the stick-slip kinematics of HDPE in a slit die, also by using LDV, was recently provided by Robert et al. (2004). These researchers reported that slip was not homogeneous across the slit die and that a pure plug flow is expected only for very high flow rates. Then, from a numerical computation, these authors suggested that the measured slip velocities were of the same order of magnitude as those measured in a capillary rheometer. Mitsoulis et al. (2005) analyzed the flow of branched polypropylene in a quartz capillary by visualization combined with laser speckle velocimetry and simulation. These authors showed the formation of vortices in the contraction region and suggested their variation in size with increasing shear rate to be related to the presence of slip. The reported velocity profiles, however, do not exhibit slip. Finally, Rodríguez-González et al. (2009) described for the first time the flow kinematics of HDPE in a glass capillary die by using particle image velocimetry (PIV). These authors corroborated the main results by Münstedt et al. (2000) and Robert et al. (2004) and showed that the velocity profiles cannot become plug like in the presence of shear thinning in the melt. In addition, Rodríguez-González et al. provided a proof for the basic assumption of the Mooney method by comparing velocity profiles obtained under slip and no slip flow conditions.

The aim of this work is to describe the kinematics as well as the dependence of the slip velocity on shear stress during the capillary flow of a metallocene LLDPE (mLLDPE). To accomplish this goal, the 2D PIV technique has been coupled with rheometrical measurements (rheo-PIV). PIV has been seldom used in the study of the flow of polymer melts (see Nigen et al. 2003) but has been successfully applied for the analysis of the capillary flow of shear banding micellar solutions, (Méndez-Sánchez et al. 2003; Marín-Santibáñez et al. 2006) and very recently to study the stick-slip capillary flow of HDPE (Rodríguez-González et al. 2009).

Compared with LDV, which measures the velocity at a point, PIV has the advantage that instantaneous velocity maps of the flow region may be obtained, which allow for the detection of rapid variations in a plane of the flow field. This feature of the PIV technique permits, for example, the instantaneous measurement of the slip velocity during stable and unstable flow conditions. Therefore, by using this technique, we have been able to capture most of the features (some of them not previously shown) of the flow kinematics of a mLLDPE in a capillary die in a wider range of shear rates than in previous works. Details of the research are given below.

Experimental

Materials and rheometry

The polymer used in this work was a mLLDPE (ethylene-co-1-butene, Aldrich 434698) with a relative density of 0.88, melt flow index of 0.8 g/10 min, differential scanning calorimetry peak melting point of 60°C, $M_w/M_n \sim 2$, and $M_w = 93,200$ g/mol. This polymer is reported as free of additives that might screen macromolecules interactions at the die wall.

The experiments were carried out at a temperature of 190°C under continuous extrusion with a computer-operated PL 2100 Brabender single screw extruder of 0.019 m in diameter and length to diameter ratio of 25/1. The pressure drop (Δp) between capillary ends was measured with a Dynisco™ pressure transducer, and the volumetric flow rate (Q) was determined by collecting and measuring the ejected mass as a function of time. From these data, the wall shear stress (τ_w) and the apparent shear rate ($\dot{\gamma}_{app}$) were calculated as:

$$\tau_w = \frac{\Delta p}{\left(4 \frac{L}{D}\right)} \quad (1)$$

$$\dot{\gamma}_{app} = \frac{32Q}{\pi D^3} \quad (2)$$

where L and D are the length and diameter of the capillary, respectively.

Previous measurements performed with mLLDPE and dies of different L/D ratios suggest that an $L/D = 20$ is enough to reach a fully developed flow and to make end effects negligible (Pérez-González et al. 2000). Therefore, a capillary die ($D = 0.00171$ m) made up of borosilicate glass, with an entry angle of 180° and $L/D = 20$, was adapted to the extruder to carry out the measurements, and no corrections for end effects were performed. This type of glass capillaries has more than

90% of light transmissibility, high resistance to wear, and high dimensional stability under several processing conditions. They have been successfully tested in previous rheometrical and PIV studies with polymer melts and have been proved to produce reliable results (Pérez-González and de Vargas 1999; Rodríguez-González et al. 2009).

Slip and no slip flow conditions were investigated. Strong slip conditions at the die wall were promoted with a fluoropolymer polymer processing additive (FPPA) Dynamar™ FX-9613 added to the mLLDPE in a concentration of 0.1 wt.% (see Migler et al. 2001). The FPPA is immiscible in the mLLDPE and migrates to the die wall under flow, producing a slippery layer or interfacial slip between the polymer melt and the FPPA. A detailed study of the die coating process and the necessary thickness to eliminate sharkskin using this FPPA has been performed by Kharchenko et al. (2003). Slip flow was recognized by the disappearance of sharkskin distortions, by a decrease in the pressure drop at constant screw speed, and by the presence of electric charge on the extrudates (see Pérez-González and Denn 2001; Pérez-González 2001). The induction time (time to achieve strong slip conditions) was set to 2.5 h of flow at 4 rpm. This time may change depending on the imposed apparent shear rate and the cleanness of the die internal surface. Increasing the flow rate and cleanness of the die wall results in shorter induction times. Cleaning of the extrusion system was performed with Unipurge™ before each experiment.

PIV measurements

The study of the flow kinematics in the capillary was performed with a 2D PIV Dantec Dynamics system as sketched in Fig. 1. The 2D PIV technique provides

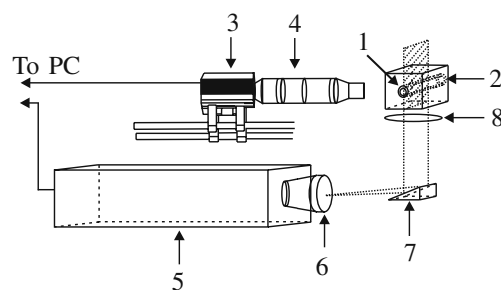


Fig. 1 Schematic representation of the experimental set up. (1) Capillary, (2) aberration corrector, (3) CCD camera, (4) microscope, (5) lasers, (6) cylindrical lens, (7) prism, (8) biconvex lens

instantaneous measurements of the velocity vectors in a plane of the flow field (velocity maps). Full description of the PIV technique and the experimental set up are presented elsewhere (Rodríguez-González et al. 2009). Therefore, only a brief account of this part of the experimental protocol is presented here.

The PIV system utilized consists of a high speed and high sensitivity HiSense MKII charge-coupled device (CCD) camera of 1.35 megapixels, two coupled Nd/YAG lasers of 50 mJ with $\lambda = 532$ nm, and the Dantec Dynamic Studio 2.1 software. Solid copper spheres <10 μm in diameter (Aldrich 32,6453) at a concentration of 0.5 wt.% were used for seeding. This amount of particles does not affect the rheological behavior of the polymer (Rodríguez-González et al. 2009).

The observation plane was reduced in thickness up to less than 200 μm and made to coincide with the center plane of the capillary. An InfiniVar™ continuously focusable video microscope CFM-2/S was attached to the CCD camera in order to increase the spatial resolution. The depth of field of the microscope at the position of observation was measured as 40 μm . A small depth of field reduces the true observation volume and the error introduced by out-of-plane particles (the observation region is not really a plane, since the light sheet has a finite width). This fact is particularly important in experiments where the shear stress distribution is not homogeneous, since the wider the light sheet, the bigger the variation of the shear stress in the observation volume. Thus, the variation of the shear stress in the region associated with the depth of field of the microscope in this work was only 5% of τ_w .

Image distortion due to curvature of the capillary wall was eliminated by using an aberration corrector, which was made up of a small rectangular prism with glass walls as shown in Fig. 1. For this purpose, the refractive index (n) of the borosilicate glass capillary ($n_{\text{glass}} = 1.43$) was closely matched by filling the prism with glycerol ($n_{\text{gly}} = 1.47$). In order to make the PIV measurements, one part of the capillary corresponding to a length of $15D$ was kept inside the extruder die head at controlled temperature, and the rest of the capillary was inside the aberration corrector, in which the temperature was continuously monitored and supplied with glycerol at the desired temperature.

The images taken by the PIV system covered an area of 0.00171×0.0032 m and were centered at an axial position $z = 17D$ downstream from the contraction. Series of 50 image pairs were obtained for each flow condition. The time between consecutive images was changed according to the imposed shear rate and ranged from

50 μs for 616 s^{-1} up to 0.006 s at 42.6 s^{-1} . The image acquisition frequency was fixed at 6.1 Hz under stable flow in order to obtain full camera resolution; thus, the total acquisition time for the 50 photographs was 8.19 s. The acquisition frequency was reduced to 2.0 Hz during the stick-slip due to the relatively slow pressure oscillations observed.

For the stable flow conditions, all the image pairs were interrogated and ensemble averaged to obtain a single velocity map. This was not made for the stick-slip regime where the velocity oscillates with time. The axial velocity component as a function of the radial position (velocity profile) was obtained by averaging the profiles in a map.

An adaptive correlation algorithm with a central difference approximation was used to calculate the velocity vectors. This technique has been proved to be more accurate than conventional PIV algorithms when measuring near flow boundaries or in the presence of velocity gradients (Wereley and Meinhart 2001), which is the case during the evaluation of velocity vectors in the neighborhood of the capillary wall. Each interrogation window was chosen as a rectangle of 256 pixels long and 16 pixels wide (642×40 μm , radial and axial direction, respectively), with an overlap of 50% in both axis. With this size of the interrogation area and the type of particles used for seeding, the closest distance to the capillary wall at which we could measure was 40 μm . Further approach to the wall would require the seeding with smaller particles. Finally, data validation was performed by using a moving average filter.

Results and discussion

Rheometry and analysis of the flow curves

The flow curves for the mLLDPE with and without additive are shown in Fig. 2. The flow curve corresponding to the pure polymer is typical of a melt exhibiting stick-slip instabilities; only regions I–II were explored. Region I corresponds to a stable flow regime that cannot be well fitted by a simple power law. Instead, a more complex constitutive equation seems to describe the melt behavior. Earlier works used to attribute deviations of LLDPEs from the power law (slope change) to the presence of slip (see for example Kalika and Denn 1987). Nevertheless, as it is shown below by the velocimetry analysis, this is not necessarily the case. Shaw (2007) has recently showed that a constitutive equation more complex than a power law may

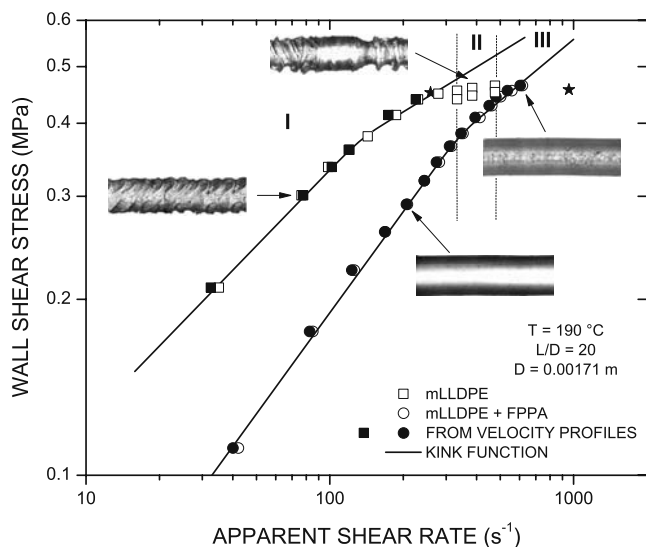


Fig. 2 Flow curves for the mLLDPE with and without FPPA. Filled symbols correspond to data obtained by PIV. The star symbols correspond to the apparent shear rates calculated from the velocity profiles during one stick-slip cycle at 383.5 s⁻¹. The continuous lines represent the fitting to continuous “kink” functions

be confused with a slope change. Following this line of thought, the flow data for the pure polymer may be very well fitted by a continuous “kink” function of type II (Shaw 2007), namely:

$$\log \tau_w = 5.5743 + 0.4307(\log \dot{\gamma}_{app} - 2.1205) + 0.0325(0.2553 - 0.4307) \times \ln \left\{ 1 + \exp \left[\frac{\log \dot{\gamma}_{app} - 2.1205}{0.0325} \right] \right\} \quad (3)$$

The stick-slip instability appears in region II, where the amplitude of pressure oscillations (represented by double points) is almost independent of the imposed flow rate, except for apparent shear rates in the neighborhood of stable branches I and III.

Figure 2 includes the flow curve obtained for the mLLDPE containing additive, which is clearly different from that of the pure polymer. In this case, a flow enhancement with respect to the pure polymer is evident, as well as the absence of the stick-slip regime. This flow enhancement results from the interfacial slip between the polymer melt and FPPA. In addition, the flow curves become one beyond the stick-slip regime, which suggests that bulk effects dominate over surface interactions at high apparent shear rates. It is noteworthy here that the flow curve for the mLLDPE containing

additive also deviates from a power law and can be very well fitted by a continuous “kink” function of type II:

$$\log \tau_w = 5.5823 + 0.5743(\log \dot{\gamma}_{app} - 2.513) + 0.0278(0.3475 - 0.5743) \times \ln \left\{ 1 + \exp \left[\frac{\log \dot{\gamma}_{app} - 2.513}{0.0278} \right] \right\} \quad (4)$$

On the other hand, in agreement with the description in the previous paragraph, the difference in the morphology of the extrudates was remarkable; while those obtained by using FPPA (strong slip conditions) only showed gross melt fracture at high shear rates, the pure polymer (no slip) exhibited the well known succession of defects, namely, sharkskin followed by stick slip (see the inserts in Fig. 2).

The slip velocity (v_s) for the mLLDPE + FPPA system was calculated by comparing the data from both flow curves in Fig. 2 using the equation:

$$v_s = \frac{4(Q_s - Q_{f-s})}{\pi D^2} \Big|_{\tau_w} \quad (5)$$

where Q_s and Q_{f-s} represent the volumetric flow rates with slip and free of slip, respectively, for a given τ_w . Note that Eq. 5 represents the basic assumption of the Mooney (1931) method, which is a phenomenological correction representing the contribution of slip to the experimentally measured flow rate. To use this equation, only stable data from the pure polymer before the stick-slip were considered, assuming them as free of slip (the proof for this assumption is provided in the next section). The slip velocity as a function of the shear stress is shown in Fig. 3.

The slip velocity increases with the shear stress and follows a power law behavior at low shear stresses, but the trend changes as the shear stress is further increased. This change of the rate of increase of the slip velocity along with the shear stress has been attributed to shear thinning of the melt (Pérez-González and de Vargas 2002; Pérez-Trejo et al. 2004) in agreement with the predominance of bulk effects over surface interactions at the die wall.

Velocity measurements by using PIV

Pure mLLDPE

Region I The velocity maps for the different shear rates in the low shear rate branch for the pure polymer are shown in Fig. 4. There is not a significant change of the velocity profiles inside the observation region, and the radial component of the velocity was two orders

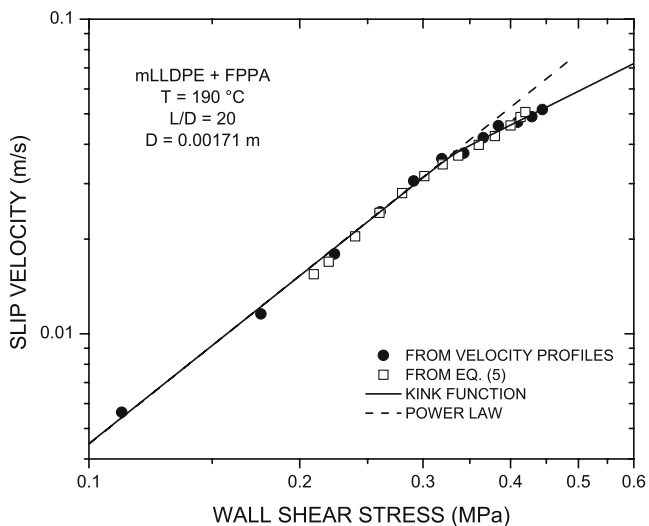
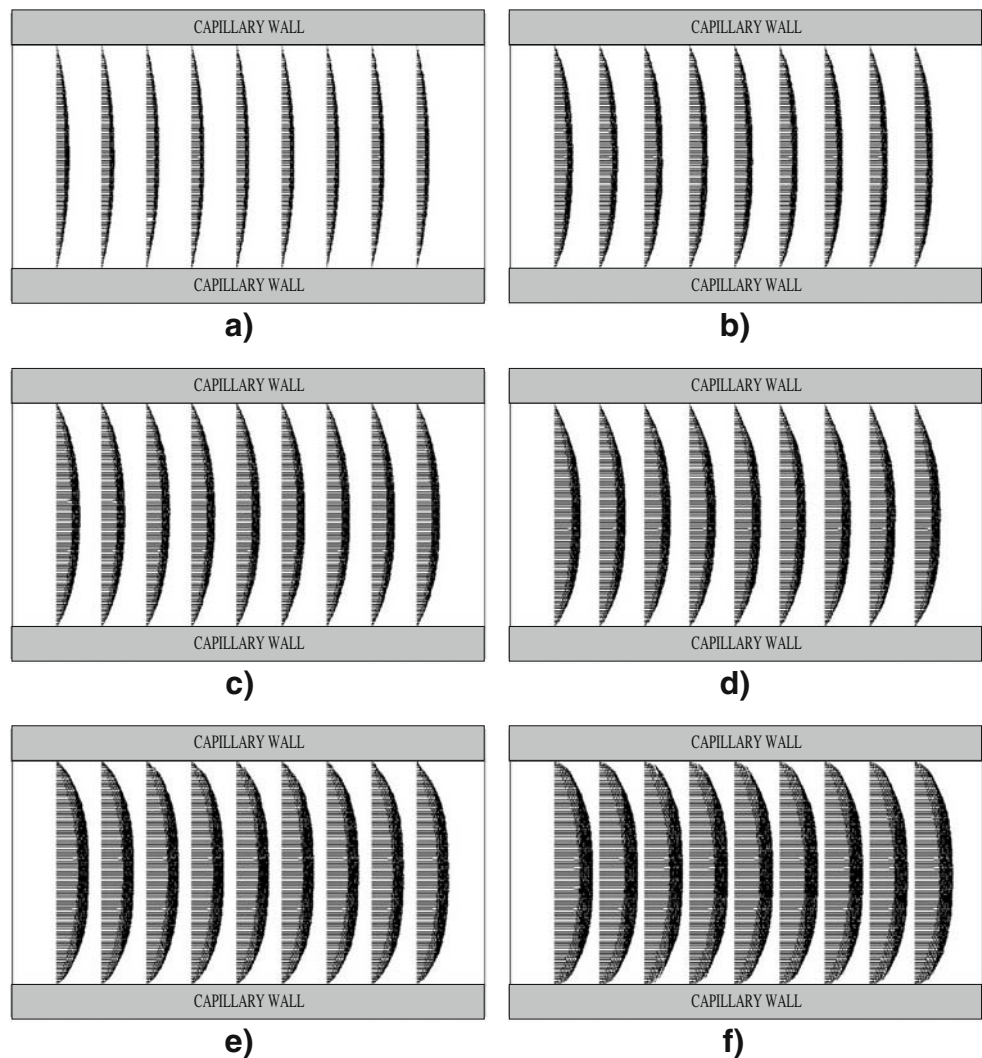


Fig. 3 Slip velocity as a function of the shear stress for mLLDPE + FPPA. *Filled symbols* correspond to data obtained directly from the velocity profiles. The *continuous line* represents the fitting to a continuous “kink” function and the *dashed one* to a power law

Fig. 4 Velocity maps for the different apparent shear rates in the low shear rate branch for the pure mLLDPE: **a** 35.4 s^{-1} , **b** 76.5 s^{-1} , **c** 98.8 s^{-1} , **d** 120.6 s^{-1} , **e** 187.5 s^{-1} , **f** 232.8 s^{-1}



of magnitude smaller than the axial one in each case. Hence, the flow is unidirectional and the velocity field is simply given by $v_z = v_z(r)$ for the different shear rates, as it is expected for a fully developed shear flow.

Figure 5 shows the velocity profiles for the different apparent shear rates in region I. The flow rate data obtained from the integration of these velocity profiles are included in the flow curve in Fig. 2 in order to validate the PIV results. There is a very good agreement between the rheometrical and PIV data in region I. The differences in the volumetric flow rates obtained by the two methods are less than 7%, which shows the reliability of the velocimetry technique. However, according to the discussion in the previous section, a single power law relationship was not appropriate to describe all of these profiles (see Fig. 2). This is in contrast with the results by Migler et al. (2001), who described the velocity profiles of a mLLDPE by using a power law function.

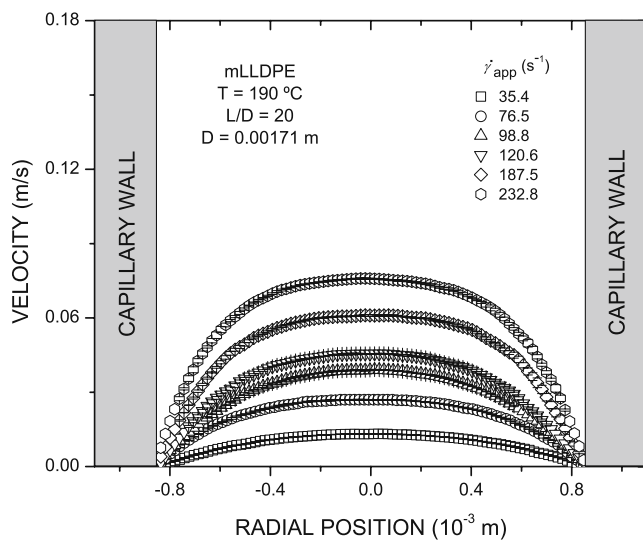


Fig. 5 Velocity profiles for the different apparent shear rates in the low shear rate branch of the pure mLLDPE. The lines inside the symbols correspond to error bars

Note that the velocity profiles in this flow regime extrapolate to a zero value at the die wall (no slip), which supports the assumption made in using Eq. 5. The absence of slip agrees with the results by Migler et al. (2001) for a comparable melt index mLLDPE. As it is known, the critical shear stress and the magnitude of slip depend on the polymer molecular weight (Hatzikiriakos and Dealy 1992; Wang 1999). The higher the M_w , the smaller the critical stress for slip and the larger v_s .

Region II Figure 6 shows two velocity profiles during a pressure oscillation for the apparent shear rate of 383.5 s^{-1} (region II). These velocity profiles exhibit the alternation of the boundary condition at the die wall, which is characteristic of the stick-slip flow regime. The velocity in the maximum profile (slip) is more than twice the minimum (stick), and the slip velocity during the spurt reaches 63% of the maximum velocity in the slip profile. The apparent shear rates corresponding to these profiles are included as star symbols in Fig. 2. It is interesting to note that the second star does not lie on region III of the flow curve. This is due to the fact that the amplitude of pressure oscillations is not constant, and there are occasional large spurts for which the integrated flow rate lies out of region III. The data included in Fig. 2 correspond, by chance, to a stick-slip cycle with one of such large spurts. Similar behavior has been observed in PIV measurements of other spurling materials as molten HDPE (Rodríguez-González et al. 2009) and wormlike micellar solutions (Méndez-Sánchez et al. 2003). In the HDPE, for instance, the

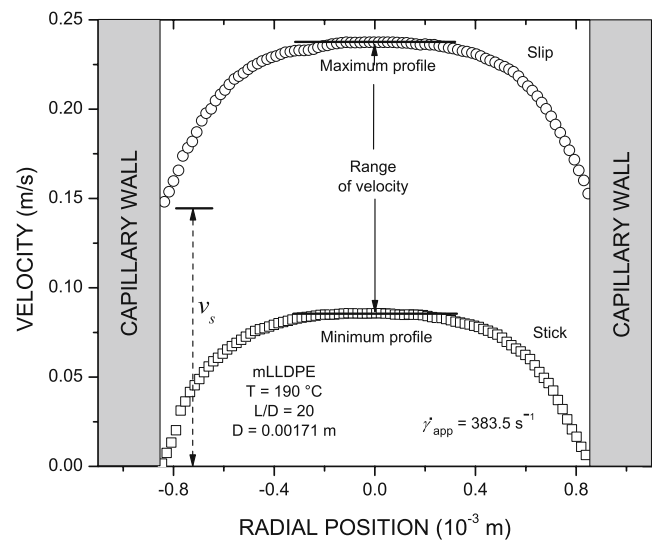


Fig. 6 Minimum and maximum velocity profiles during one stick-slip oscillation of mLLDPE at an apparent shear rate of 383.5 s^{-1} . The apparent shear rates corresponding to these profiles are the star symbols appearing in Fig. 2

flow rate during pressure oscillations may reach values that lie short from region I of the flow curve (see Fig. 2 in Rodríguez-González et al. 2009).

A detailed description of the flow kinematics in the stick-slip regime of HDPE was recently provided by Rodríguez-González et al. (2009). The results for this mLLDPE conform to those in the previously mentioned report. However, an issue to highlight in the analysis of the stick-slip flow of this metallocene is the appearance of nonhomogeneous slip (Fig. 7a), i.e., the simultaneous appearance of regions with and without slip at the die wall. This new characteristic of the stick-slip flow was recently discovered by Rodríguez-González et al. (2009) in HDPE, and it is nicely visualized in the photograph of the extrudate in Fig. 7b. It is noteworthy that these peculiar details of the stick-slip flow may only be detected by instantaneous measurements of the flow field.

Rodríguez-González et al. (2009) related this phenomenon of nonhomogeneous slip to the partial slip reported by Ghanta et al. (1999) and Pérez-González and Denn (2001) for LLDPE. Nevertheless, a detailed tracking of the defect along the mLLDPE extrudates for different apparent shear rates in region II (which is not easy to do in HDPE since sharkskin is typically absent) permitted its detection in different parts on the extrudates periphery. The fact that the nonhomogeneous slip alternates on the extrudates periphery suggests that it might be related to a sort of swirling motion or oscillation upstream of the die. Such upstream instabilities have been reported for extrusion in

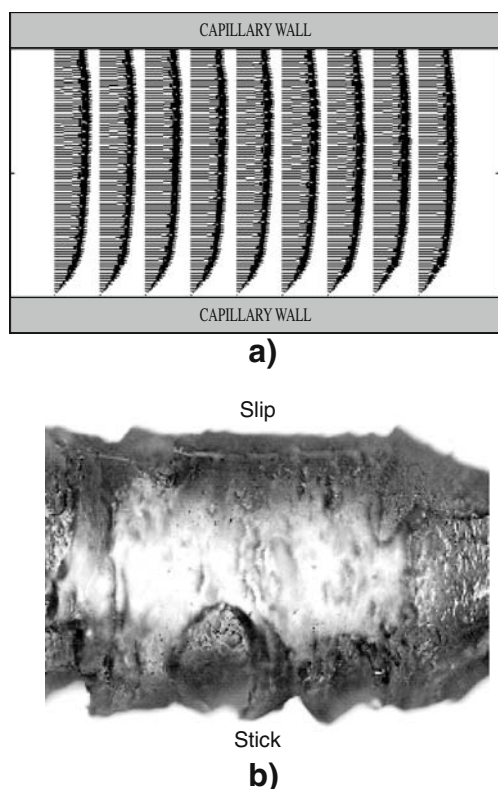


Fig. 7 **a** Velocity map and **b** extrudate displaying nonhomogeneous slip during the stick slip of mLLDPE

the melt fracture regime (Kazatchkov et al. 2000; Nigen et al. 2003; Combeaud et al. 2007) and may indeed give rise to pressure oscillations (Pérez-González et al. 1997) but are not characteristic of the stick-slip regime. Moreover, the frequency of apparition of nonhomogeneous slip is much higher than that reported by the above-mentioned authors for upstream instabilities and also than the one due to the rotation of the screw, which would rule out this phenomenon as due to an upstream instability. Further work including the visualization of the upstream and downstream regions is necessary to clarify this point.

mLLDPE + FPPA

The slip velocity Figure 8a, b shows the velocity profiles obtained for the mLLDPE under strong slip conditions. In contrast to the observed for the pure polymer, the velocity profiles in Fig. 8a, b exhibit a nonzero velocity at the die wall, whose magnitude increases along with the apparent shear rate (shear stress). Note, however, that the slip velocity seems to increase more slowly at the highest shear rates studied. The slip velocity values obtained from the extrapolation of the velocity profiles at the die wall are plotted in Fig. 3

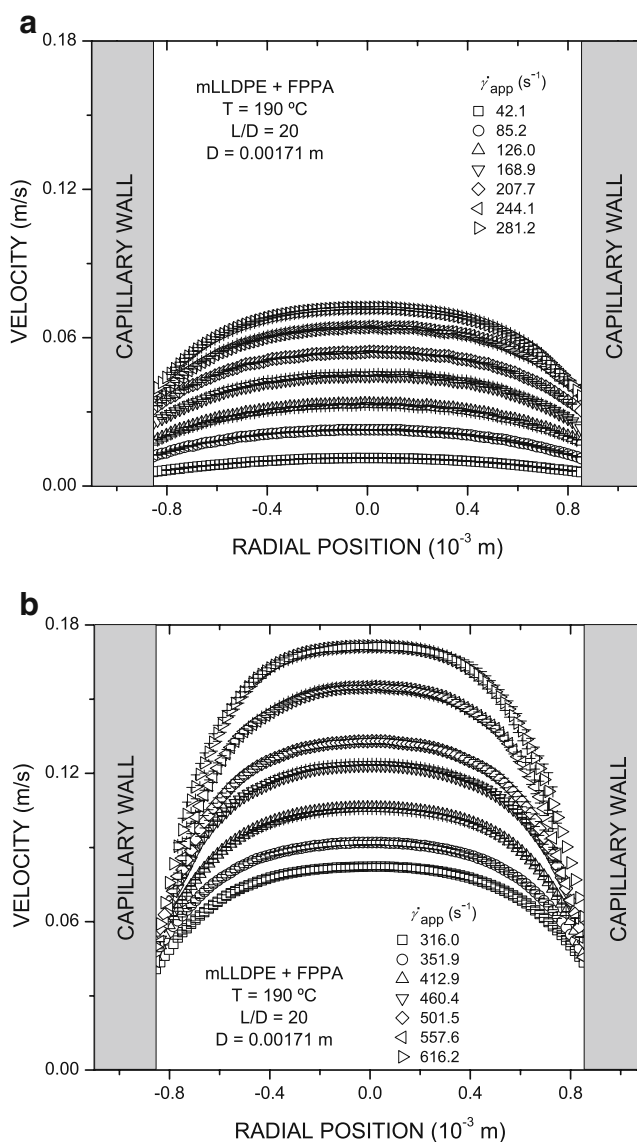


Fig. 8 Velocity profiles obtained at different apparent shear rates for mLLDPE + FPPA: **a** 42.1, 85.2, 126.0, 168.9, 207.7, 244.1, and 281.2 s⁻¹; **b** 316.0, 351.9, 412.9, 460.4, 501.5, 557.6, and 616.2 s⁻¹. The lines inside the symbols represent the amplitude of error bars

along with those calculated from the rheometrical data by using Eq. 5. The agreement between both sets of data is remarkable, which provides a direct proof for the validity of Eq. 5 or the basic Mooney hypothesis to evaluate the influence of slip in capillary flow (see also Rodríguez-González et al. 2009). Also, the slip velocity values in Fig. 3 and the trend as a function of the shear stress are comparable to those reported by Migler et al. (2001) at low shear stresses (<0.30 MPa) in agreement with the similar characteristics of the used polymers, FPPA, and nonmetallic dies.

The relationship between the slip velocity and wall shear stress in Fig. 3 clearly deviates from the power

law behavior at a shear stress above 0.30 MPa. Similar behavior was reported by Guadarrama-Medina et al. (2005) for a different LLDPE containing the same FPPA. Then, a more realistic equation that could be used in numerical calculations may be obtained by fitting the data to a continuous “kink” function (Shaw 2007):

$$\begin{aligned} \log v_s = & -1.4276 + 1.7716 (\log \tau_w - 5.5202) \\ & + 0.0078 (1.11 - 1.7716) \\ & \times \ln \left\{ 1 + \exp \left[\frac{\log \tau_w - 5.5202}{0.0078} \right] \right\} \end{aligned} \quad (6)$$

A comparison of the slip velocity calculated by using the kink function (6) and a power law (see Fig. 3) at $\tau_w = 0.443$ MPa (the highest shear stress reached in this work) leads to an overestimation of 23% in v_s when using the power law model. Considering the trend in Fig. 3 for the slip velocity, the error introduced by using a power law model for this polymer will become even more significant at higher shear stresses.

The ratio of slip to average velocity The ratio of v_s to average velocity ($\langle v \rangle$) is shown in Fig. 9; it exhibits a maximum at the same shear stress where v_s deviates from the power law and then decreases as the shear stress is further increased. The maximum contribution of v_s to the flow field reaches $0.69 \langle v \rangle$. The existence of a maximum in the contribution of v_s to $\langle v \rangle$ has

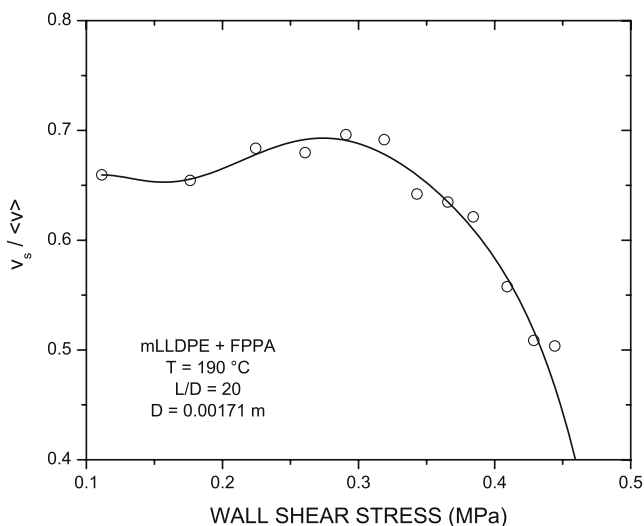


Fig. 9 Ratio of v_s to $\langle v \rangle$ for mLLDPE + FPPA

been reported, from pure rheometrical measurements, for rubber compounds by Dimier et al. (2002) and for LLDPEs by Pérez-Trejo et al. (2004) using brass dies and by Guadarrama-Medina et al. (2005) using stainless steel dies and the same FPPA. Direct measurements of the velocity profiles in this work corroborate the trend of $v_s / \langle v \rangle$ to reach a maximum. This result evidences the predominance of shear over slip flow at high shear stresses and may be interpreted as the impossibility for the velocity profile to become plug like in the presence of shear thinning. In other words, there must always be a shear contribution in the bulk that leads to the development of the velocity profile. Stronger shear thinning at high shear stresses may be due to the influence of the contraction, which results in high orientation of polymer molecules. Finally, the use of $v_s / \langle v \rangle$ has a direct significance in evaluating the influence of slip in polymer processing operations.

Conclusions

The continuous extrusion of a metallocene linear low-density polyethylene with and without slip was analyzed in this work by rheometrical measurements and particle image velocimetry. A detailed description of the flow kinematics and measurement of the slip velocity under stable and unstable flow conditions was performed. Very good agreement was found between rheometrical and PIV measurements, which shows the reliability of PIV to analyze the flow of polymer melts. The pure polymer exhibited stick-slip instabilities with nonhomogeneous slip at the die wall, but the addition of a small amount of FPPA, which induced interfacial slip, produced stable flow accompanied by a monotonic flow curve. The slip velocity was zero for the pure polymer before the stick-slip but increased monotonously as a function of the shear stress for the polymer containing FPPA. The dependence of the slip velocity on the shear stress deviated from a power law and was well fitted by a continuous “kink” function. A direct proof of the basic assumption of the Mooney theory was made by direct comparison of PIV data with rheometrical ones. A maximum was found in the contribution of slip to the average fluid velocity, which was interpreted as the impossibility for the velocity profile to become plug like in the presence of shear thinning.

Acknowledgements This research was supported by SIP-IPN (20091012). F. R-G. and B. M. M-S. had CONACYT and PIFI-IPN scholarships to carry out this work. J. P-G. and L. de V. are COFFA-EDI fellows.

References

- Atwood BT, Schowalter WR (1989) Measurements of slip at the wall during flow of high-density polyethylene through a rectangular conduit. *Rheol Acta* 28:134–146
- Combeaud C, Vergnes B, Merten A, Hertel D, Münstedt H (2007) Volume defects during the extrusion of polystyrene investigated by flow induced birefringence and laser-Doppler velocimetry. *J Non-Newton Fluid Mech* 145:69–77
- Denn MM (2001) Extrusion instabilities and wall slip. *Ann Rev Fluid Mech* 33:265–287
- Dimier F, Vergnes B, Vincent M (2002) Le glissement à la paroi d'un mélange de caoutchouc naturel. *Réologie* 1:35–39
- El Kissi N, Piau JM (1996) Slip and friction of polymer melt flows. In: Piau JM, Agassant JF (eds) *Rheology for polymer melt processing*. Elsevier, New York, pp 357–388
- Ghanta VG, Riise BL, Denn MM (1999) Disappearance of extrusion instabilities in brass capillary dies. *J Rheol* 43:435–442
- Guadarrama-Medina TJ, Pérez-González J, de Vargas L (2005) Enhanced melt strength and stretching of linear low-density polyethylene extruded under strong slip conditions. *Rheol Acta* 44:278–286
- Hatzikiriakos SG, Dealy JM (1992) Wall slip of molten high density polyethylenes, II. Capillary rheometer studies. *J Rheol* 36:703–741
- Joshi JN, Lele AK, Mashelkar RA (2000) Slipping fluids: a unified transient network model. *J Non-Newton Fluid Mech* 89:303–335
- Kalika DS, Denn MM (1987) Wall slip and extrudate distortion in linear low-density polyethylene. *J Rheol* 31:815–834
- Kazatchkov IB, Yip F, Hatzikiriakos SG (2000) The effect of boron nitride on the rheology and processing of polyolefins. *Rheol Acta* 39:583–594
- Kharchenko SB, McGuiggan PM, Migler KB (2003) Flow induced coating of fluoropolymer additives: development of frustrated total internal reflection imaging. *J Rheol* 47:1523–1545
- Leonov AI (1990) On the dependence of friction force on sliding velocity in the theory of adhesive friction of elastomers. *Wear* 141:137–145
- Malkin YA (2006) Flow instability in polymer solutions and melts. *Polym Sci Ser C* 48:21–37
- Malkin YA (2009) The state of the art in the rheology of polymers: achievements and challenges. *Polym Sci Ser A* 51:80–102
- Marín-Santibáñez BM, Pérez-González J, de Vargas L, Rodríguez-González F, Huelsz G (2006) Rheometry-PIV of shear-thickening wormlike micelles. *Langmuir* 22:4015–4026
- Méndez-Sánchez AF, Pérez-González J, de Vargas L, Castrejón-Pita JR, Castrejón-Pita AA, Huelsz G (2003) Particle image velocimetry of the unstable capillary flow of a micellar solution. *J Rheol* 47:455–1466
- Migler KB, Lavallée C, Dillon MP, Woods SS, Gettinger CL (2001) Visualizing the elimination of sharkskin through fluoropolymer additives: coating and polymer–polymer slippage. *J Rheol* 45:565–581
- Mitsoulis E, Kazatchkov IB, Hatzikiriakos SG (2005) The effect of slip in the flow of a branched PP melt: experiments and simulations. *Rheol Acta* 44:418–426
- Mooney M (1931) Explicit formulas for slip and fluidity. *J Rheol* 2:210–222
- Müller-Mohnssen H, Löbl HP, Schauerte W (1987) Direct determination of apparent slip for a ducted flow of polyacrylamide solutions. *J Rheol* 31:323–336
- Münstedt H, Schmidt M, Wassner E (2000) Stick and slip phenomena during extrusion of polyethylene melts as investigated by laser-Doppler velocimetry. *J Rheol* 44:413–427
- Nigen S, El Kissi N, Piau JM, Sadum S (2003) Velocimetry field for polymer melts extrusion using particle image velocimetry stable and unstable flow regimes. *J Non-Newton Fluid Mech* 112:177–202
- Pérez-González J (2001) Exploration of the slip phenomenon in the capillary flow of linear-low density polyethylene via electrical measurements. *J Rheol* 45:845–853
- Pérez-González J, de Vargas L (1999) On the rheological characterization of polyethylene melts by using glass capillaries. *Polym Test* 18:397–403
- Pérez-González J, de Vargas L (2002) Quantification of the slip phenomenon and the effect of shear thinning in the capillary flow of linear polyethylenes. *Polym Eng Sci* 42:1231–1237
- Pérez-González J, Denn MM (2001) Flow enhancement in the continuous extrusion of linear low-density polyethylene. *Ind Eng Chem Res* 40:4309–4316
- Pérez-González J, Pérez-Trejo L, de Vargas L, Manero O (1997) Inlet instabilities in the capillary flow of polyethylene melts. *Rheol Acta* 36:677–685
- Pérez-González J, de Vargas L, Pavlínek V, Hausnerová B, Sába P (2000) Temperature-dependent instabilities in the capillary flow of a metallocene linear low-density polyethylene melt. *J Rheol* 44:441–451
- Pérez-Trejo L, Pérez-González J, de Vargas L, Moreno E (2004) Triboelectrification of molten linear low-density polyethylene under continuous extrusion. *Wear* 257:329–337
- Piau JM, El Kissi N (1994) Measurement and modelling of friction in polymer melts during macroscopic slip at the wall. *J Non-Newton Fluid Mech* 54:121–142
- Piau JM, Kissi N, Mezghani A (1995a) Slip flow of polybutadiene through fluorinated dies. *J Non-Newton Fluid Mech* 59:11–30
- Piau JM, El Kissi N, Toussant F, Mezghani A (1995b) Distortions of polymer melt extrudates and their elimination using slippery surfaces. *Rheol Acta* 34:40–57
- Ramamurthy AV (1986) Wall slip in viscous fluids and influence of materials of construction. *J Rheol* 30:337–357
- Reiner M (1931) Slippage in a non-Newtonian liquid. *J Rheol* 2:338–349
- Robert L, Demay Y, Vargnes B (2004) Stick-slip flow of high density polyethylene in a transparent slit die investigated by laser Doppler velocimetry. *Rheol Acta* 43:89–98
- Rodríguez-González F, Pérez-González J, Marín-Santibáñez BM, de Vargas L (2009) Kinematics of the stick-slip capillary flow of high-density polyethylene. *Chem Eng Sci* 64:4675–4683
- Rofe CJ, de Vargas L, Pérez-González J, Lambert RK, Callaghan PT (1996) Nuclear magnetic resonance imaging of apparent slip effects in xanthan solutions. *J Rheol* 40:1115–1128
- Shaw M (2007) Determination of multiple flow regimes in capillary flow at low shear stress. *J Rheol* 51:1303–1318
- Wang SQ (1999) Molecular transitions and dynamics at polymer/wall interfaces: origins of flow instabilities and wall slip. *Adv Polym Sci* 138:227–275
- Wereley ST, Meinhart CD (2001) Second-order accurate particle image velocimetry. *Exp Fluids* 31:258–268